

Experimental Investigation of Gas Evolution in Electrochemical Discharge Machining Process

Weidong Tang, Xiaoming Kang*, Wansheng Zhao

School of Mechanical Engineering, State Key Laboratory of Mechanical System and Vibration, Shanghai Jiao Tong University, Shanghai, 200240, China

*E-mail: xmkang@sjtu.edu.cn

Received: 2 August 2018 / *Accepted:* 12 November 2018 / *Published:* 30 November 2018

Electrochemical discharge machining (ECDM) is a non-traditional processing technology used to machine non-conductive materials, such as glass and ceramics, based on electrochemical discharge phenomena around the tool electrode. The gas film is crucial in both discharge generation and machining processes. However, the characteristics of the gas film are not yet completely understood. The gas film evolution mechanisms and relationships between the gas film status and current signals need to be further investigated. In this study, a high-speed imaging technology was employed to investigate the evolution process of the gas film around the tool electrode. In addition, effects of current pulses on the gas film status were investigated. Experimental results showed that a large bubble was generated around the electrode owing to the gas production and bubble coalescence before the formation of a complete gas film. Observations of effects of current pulses on the gas film indicate that the current pulses with peak values larger than 1 A during the discharge stage were the electrolysis currents. When the applied power was turned off, the initial breakage of the gas film was observed at the bottom, which then moved upwards with an average speed of 1.03 m/s.

Keywords: Electrochemical discharge; Gas film; Bubble; Current signal; High-speed imaging

1. INTRODUCTION

Electrochemical discharge machining (ECDM) is a processing technology developed in recent years, which can be applied to micromachining of non-conductive materials including glass, quartz, and ceramics [1]. These materials are widely used in the optical and semiconductor industries. However, it is difficult to machine these hard and brittle materials by conventional machining methods; in particular, it is difficult to obtain microstructures with good surface qualities and high aspect ratios. The ECDM

technology, using the heat released by the discharge to remove materials, can machine such non-conductive brittle materials in a precise and efficient manner [2,3].

The ECDM technology is based on electrochemical discharge phenomena around a tool electrode [1]. A small tool is used as the tool electrode. In contrast to EDM, the workpiece in ECDM is non-conductive; therefore, an auxiliary electrode with a large surface is needed during processing. Both electrodes are partly immersed in an appropriate electrolyte solution (typically alkali electrolyte solution such as sodium hydroxide or potassium hydroxide). In general, the tool electrode serves as the cathode, while the auxiliary electrode serves as the anode. Both electrodes are connected to constant direct-current (DC) or pulsed voltage sources.

The ECDM process consists of an electrochemical reaction process and subsequent electrochemical discharge process. The electrochemical reaction occurs once a voltage is applied and gas bubbles are produced around the tool electrode [4, 5]. High-density bubbles coalesce into a complete gas film, which serves as the dielectric between the tool electrode and electrolyte [6]. As the gas film is very thin, the electric field across the gas film reaches the order of 10^7 V/m, which ignites the discharge between the tool electrode and electrolyte [7,8]. The high temperatures generated by these discharges remove workpiece material, which reaches the critical temperature [9].

Machining with ECDM is a complex process influenced by several parameters [10, 11], wherein the gas film is crucial. The machining accuracy, efficiency, and repeatability are directly related to the quality of the gas film [12]. Kamaraj et al. reported that the overcut of microholes in ECDM is associated with the electrolyte concentration, as the gas film quality varies with the electrolyte concentration [13]. Wüthrich et al. applied ECDM for drilling of microholes and microgrooves in glasses and reported that the gas film thickness is the main limiting factor to achieve small structures [14]. In their later study, Wüthrich and Hof proposed a theoretical model for estimation of the gas film thickness and reported that the machining repeatability can be significantly improved by reducing the gas film thickness [15]. Zheng et al. applied an offset pulse voltage in ECDM by providing a constant offset voltage at the pulse-off duration, which enhanced the stability of the gas film structure and thus improved the machining efficiency without affecting the machining accuracy [16]. Yang et al. developed a spherical tool electrode, which had a smaller electrode body with a larger spherical end, to enhance the machining efficiency and accuracy by promoting electrolyte flow to the electrode end [17]. Tang et al. proposed a diamond-coated side-insulated electrode to improve the machining accuracy and surface integrity by preventing the formation of the gas film on the electrode sidewall [18].

Extensive studies, including theoretical analyses and experimental investigations, have been performed to understand the electrochemical and dynamic properties of the gas film. Basak and Ghosh developed a theoretical model for discharge generation in the gas film, in which the discharging is modelled as a switching-circuit and a current flow emerges by blowing-off of bubbles [19]. Jain et al. characterised electric properties of bubbles and estimated the bubble diameter based on the valve theory [7]. Vogt and Balzer presented an empirical relationship to correlate the bubble coverage with the current density [20]. Wüthrich et al. analysed the processes of bubble growth and coalescence on electrodes using the percolation theory. They also estimated the critical conditions (critical voltage and current density) using probability and statistical methods [6]. In their later studies, Wüthrich and Hof proposed a theoretical model for estimation of the gas film thickness and reported that a thinner gas film can be

obtained by reducing the wettability of the tool electrode [15]. They analysed normalised current–voltage characteristics and evaluated the machining situations with reference changes in current signals [12]. Allagui and Wüthrich measured the gas film life–time and gas film formation time using the wavelet analysis as a denoising method with the discrete Meyer wavelet as a base function [21]. Cheng et al. studied the gas film quality by considering the current signal and machined contour and reported that the smallest deviation in the contour dimensions can be obtained at the transition voltage [22]. Jiang et al. presented an analytical model of the gas film and reported that the bubble development and gas film evolution are significantly affected by the surface tension and density of the electrolyte [23]. However, the characteristics of the gas film are not yet understood. The transition from bubbles to a complete gas film, gas film profile during the discharge activity, and relationships between the gas film status and current signals should be further investigated.

In this study, a high-speed camera was employed to capture the whole evolution process of the gas film around the tool electrode. The relationships between the gas film status and current signals were investigated.

2. EXPERIMENTAL DESIGN

2.1 Experimental setup

Figure 1 shows the experimental setup used to capture the gas film formation around the tool electrode using a high-speed camera during the electrochemical discharge process. The experimental setup consists of ECDM and observation units. The ECDM unit includes a DC power supply, two electrodes, and electrolyte. The tool electrode is used as the cathode, while the auxiliary electrode is used as the anode. Both electrodes are semi-immersed in the electrolyte. The electrolytic cell is made of a transparent material, which is beneficial for high-speed imaging. The observation unit includes a high-speed camera (XXRapidFrame) and oscilloscope. The real-time voltage and current signals during the imaging process were recorded by the oscilloscope. Once the high-speed camera is triggered by the real-time current signal, the high-speed imaging begins.

2.2 Materials

The power supply used in the experiments provides a smooth DC power with an applied voltage of 30 V. The auxiliary electrode is a graphite plate with dimensions of 50 mm × 20 mm × 4 mm. The tool electrode is made of tungsten and has a diameter of 500 μm. The immersion depth of the tool electrode is 2 mm; the electrolyte used in the experiments is sodium hydroxide with a concentration of 6 mol/L. The experimental parameters for the electrochemical discharge high-speed imaging are shown in Table 1. The time interval between any two adjacent images and exposure time were pre-set before the experiments. The exposure time for each image was set to 100 μs. The time interval between any two adjacent images varied in the range of 0.3 ms to 3 ms for different experiments.

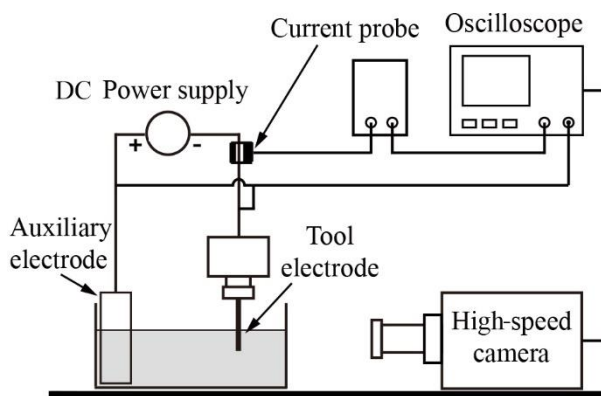


Figure 1. Experimental setup used to capture the gas film formation.

Table 1. Experimental parameters of electrochemical discharge high-speed imaging.

Factors	Parameters
Tool electrode polarity	Cathode
Tool electrode diameter	500µm
Tool electrode material	Tungsten
Tool electrode immersion depth	2mm
Electrolyte	6 mol/L NaOH
Time interval	0.3–3 ms
Exposure time	100 µs
Applied voltage	30V

2.3 Methods

When the power source was applied, gas bubbles were produced around the tool electrode due to electrolysis. The gas volume generated around the tool electrode can be calculated by:

$$V&(t) = \frac{j(t)A}{ZF} \frac{RT}{P} \tag{1}$$

where V is the total gas volume generated in electrolysis, $j(t)$ is the transferred current density, A is the contact area between the electrode and electrolyte, R is the gas constant, T is the gas temperature, Z is the valency number of altered substance, F is the Faraday constant, and P is the gas pressure. The relationship between the transferred current and transferred current density can be expressed as:

$$i(t) = j(t)A \tag{2}$$

The total gas volume produced at the time t_0 can be obtained by

$$V = \int_0^{t_0} V&(t)dt \tag{3}$$

Combining the above formulas with the current signals obtained from experiments, the total gas volume at a given time can be obtained using:

$$V = \frac{RT}{ZFP} \int_0^{t_0} i(t)dt \tag{4}$$

As the electrochemical reactions proceed, bubbles adhering to the surface of the tool electrode formed a bubble layer, as shown in Figure 2. The mean thickness of the bubble layer can be calculated as:

$$h_B = \frac{r(1) + r(2) + \dots + r(n-1) + r(n)}{n} - R \quad (n \geq 5) \tag{5}$$

where h_B is the mean thickness of the bubble layer, R is the radius of the tool electrode, and $r(n)$ is the radius of the cylinder including the tool electrode and bubble layer, as illustrated in Figure 2. The radius of the tool electrode is 250 μm . $r(n)$ can be measured from the captured bubble images according to the scale. The diameter of the largest bubble was also measured from the captured bubble images.

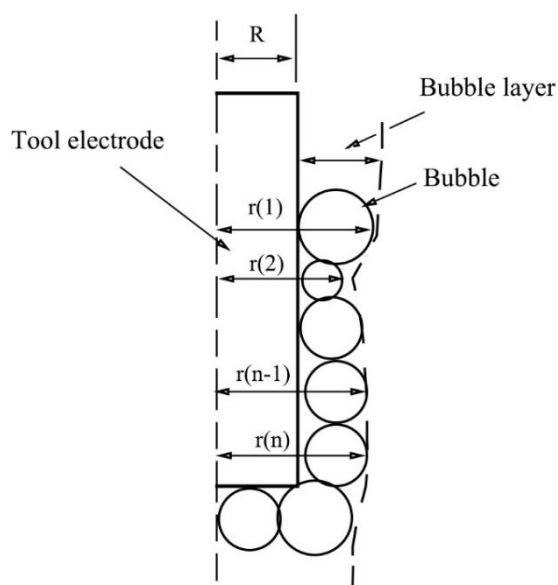


Figure 2. Bubble layer around the tool electrode.

3. RESULTS AND DISCUSSION

The ECDM process includes electrolysis and discharge processes. Bubbles are produced and coalesced into a gas film during the electrolysis process; the gas film then serves as the dielectric during the discharge process. In order to reveal the mechanisms of bubble growth and characteristics of the gas film at the discharge stage, experiments were performed to investigate the following four processes: (1) when a voltage is applied, bubble growth and development occur, (2) with the continuous growth of bubbles, high-density bubbles coalesce into a complete gas film, (3) discharge occurs around the tool electrode and the gas film is disturbed with the appearance of large current pulses at this stage, and (4) when the power is turned off, the gas film collapses. These four processes were observed and studied in sequence.

3.1 Bubble development

Figure 3 shows the evolution of bubbles around the tool electrode during the electrochemical discharge process. Figure 4 shows the corresponding voltage and current curves. The voltage applied to

the two electrodes is a DC voltage of 30 V. Point A in Figure 4 corresponds to the starting moment of the imaging acquisition; no voltage was applied at this moment. As shown in Figure 2 (a), electrolysis did not occur and there was no bubble produced around the electrode. Subsequently, the voltage was applied and the current reached a peak value of 1.27 A, as shown in Figure 4, indicating that electrolysis occurred at the contact surfaces between the tool electrode and electrolyte. Therefore, hydrogen bubbles were generated around the tool electrode, as shown in Figure 3 (b). The bubbles generated within 1 ms were small and their individual shapes were not obvious. However, at 3 ms, Figure 3 (c) shows obvious bubbles produced around the electrode. At 6 ms, the bubbles continued to coalesce and grow around the electrode, as shown in Figure 3 (d). With the progress of this process, further coalescences occur around the electrode, particularly at the bottom of the electrode, leading to the generation of large bubbles, as shown in Figure 3 (e) and 3 (f). This occurs as the bottom part of the electrode, located deeper in the solution, was subjected to a larger pressure. Therefore, bubble coalescences were easier to occur at the electrode bottom.

The evolution of bubbles around the tool electrode shows that two simultaneous processes contribute to the growth of bubbles. One of them is the increase in gas volume owing to electrolysis. The current signals in Figure 4 show that the electrolysis process lasted approximately 12 ms. The other process is the coalescence of adjacent bubbles. As shown in Figure 3 (c)–(f), the number of bubbles around the electrode decreased owing to the continuous bubble coalescence. Similar phenomena were observed in previous studies [23–26]. However, the geometrical features of the bubbles and bubble layer evolution with time have not been studied.

The growth of a single bubble at the electrode due to the electrolysis is governed by the following differential equation [23]

$$R\ddot{R} + \frac{3}{2}\dot{R}^2 = \frac{1}{\rho} \left(p - p_{\infty} - \frac{2\sigma}{R} \right) \quad (6)$$

where $R(t)$ is the growing bubble radius as a function of time, ρ is the density of the electrolyte, p is the internal pressure of the bubble, p_{∞} is the ambient pressure, and σ is the surface tension coefficient. The above equation describes the development of a single bubble owing to electrolysis. However, in the actual ECDM process, both electrolysis and bubble coalescence contribute to the bubble development, which makes the process more complex.

In order to analyse the effects of the electrolysis and bubble coalescence on the geometrical features of the bubbles and bubble layer, the gas volume, thickness of the bubble layer, and diameter of the largest bubble were calculated or measured. As mentioned above, the largest bubble usually appeared at the bottom of the electrode. The diameter of the largest bubble and mean thickness of the bubble layer were measured for each image. The measurement method was described in section 2.3. The gas volume was calculated according to Equation (4) and current signals in Figure 4.

Figures (a)–(c) show the evolution curves of the gas volume, thickness of the bubble layer, and maximum bubble diameter, respectively. Figure 5 (a) shows that the gas volume produced by the electrolysis increased approximately linearly with the time in the range of 0 ms to 12 ms. The gas volume increased to 1.1 mm³ at 12 ms. Figure 4 shows that the current value, with a slowly decreasing trend, is larger than 0.6 A within the initial 10 ms, indicating that the electrolysis continued, leading to the increase in the gas volume.

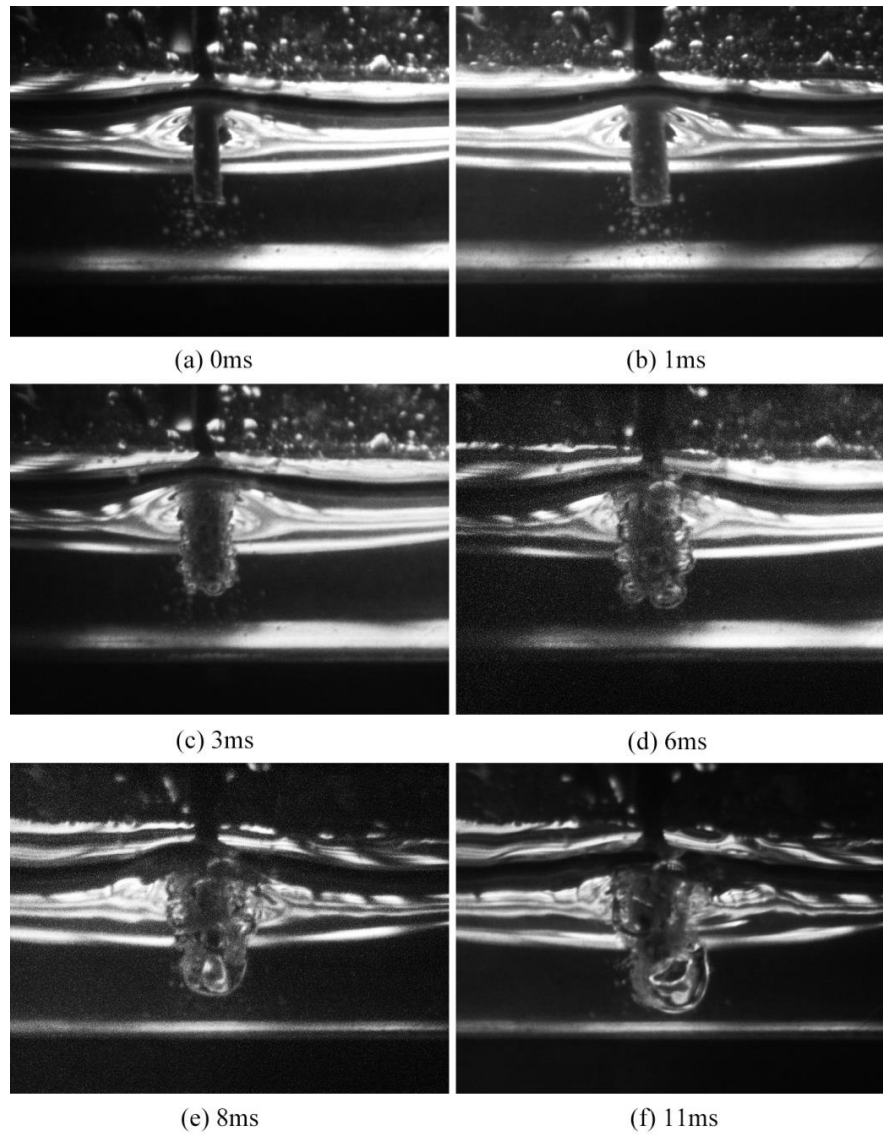


Figure 3. Bubbles evolution around the tool electrode under an applied voltage of 30V.

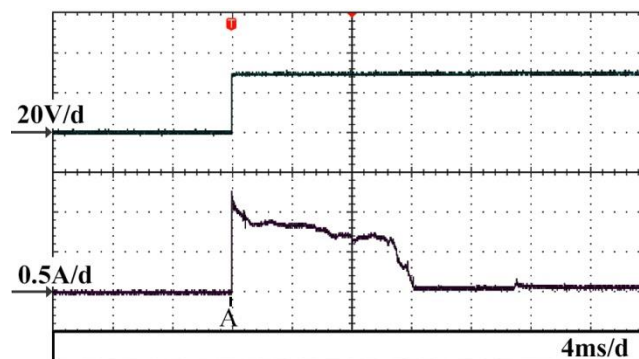


Figure 4. Voltage and current waveforms for bubbles generation.

Even though the gas volume increased linearly with time, the thickness of the bubble layer and maximum bubble diameter exhibited different behaviours, as shown in Figures 5 (b) and 5 (c),

respectively. The curve of the thickness of the bubble layer can be divided into two stages. At the stage of 0–8 ms, the thickness of the bubble layer rapidly increased. However, it exhibited a relatively slow increase in the following 4 ms. The thickness of the bubble layer increased to 660 μm at 12 ms. Similarly, the curve of the maximum bubble diameter exhibits a large change around 8 ms. The maximum bubble diameter increased slowly at the initial 8 ms and then increased from 770 μm to 1470 μm within the following 1 ms, indicating that bubble coalescence occurred at approximately 8 ms. The coalescence of the bubbles led to a denser gas, and thus the thickness of the bubble layer slowly increased after 8 ms.

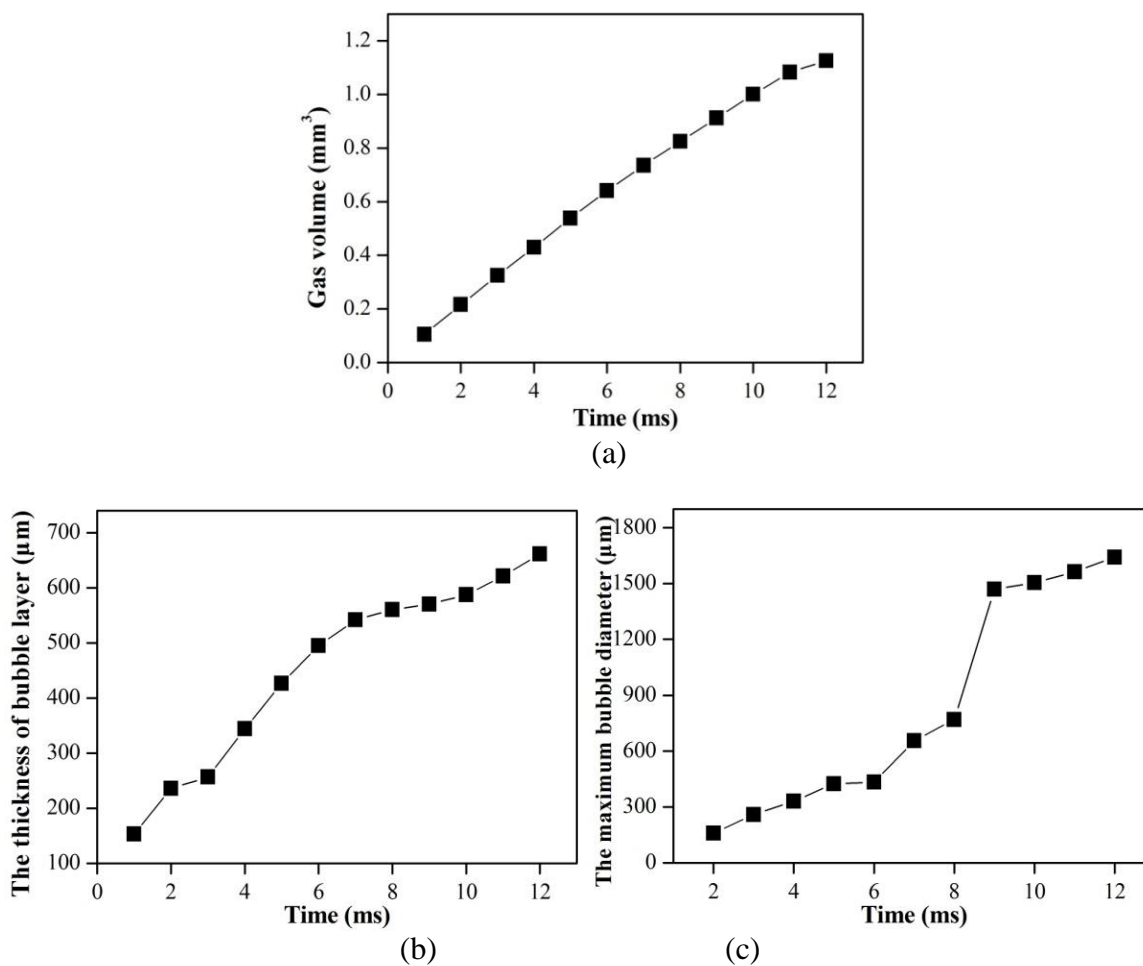


Figure 5. Temporal variations of the (a) gas volume, (b) thickness of the bubble layer, and (c) maximum bubble diameter. Experimental conditions: applied voltage: 30 V, tool electrode diameter: 500 μm , tool electrode immersion depth: 2 mm, electrolyte: 6 mol/L NaOH.

3.2 Gas film formation

When the applied voltage is higher than the critical voltage, a large number of bubbles are produced around the tool electrode. The bubbles eventually coalesce to form a complete gas film around the tool electrode, as observed in previous studies [23-26]. However, the previous studies focused on investigation of the bubble state or gas film state. A complete stable gas film is necessary for a stable

discharging. Therefore, it is of interest to investigate the transformation of bubbles into a complete gas film.

Figure 6 shows the process of bubble transformation into a complete gas film under an applied voltage of 30 V. Figure 7 shows the corresponding voltage and current waveforms. The high-speed imaging began at point A and ended at point F, as shown in Figure 7. The current at point A was 310 mA; the corresponding image is shown in Figure 5 (a), which shows a large ellipsoidal bubble around the electrode. The large bubble indicates that the bubble coalescence continued with time, and finally the bubbles coalesced into one large bubble. The current simultaneously decreased during the bubble coalescence process, as shown in Figure 7..

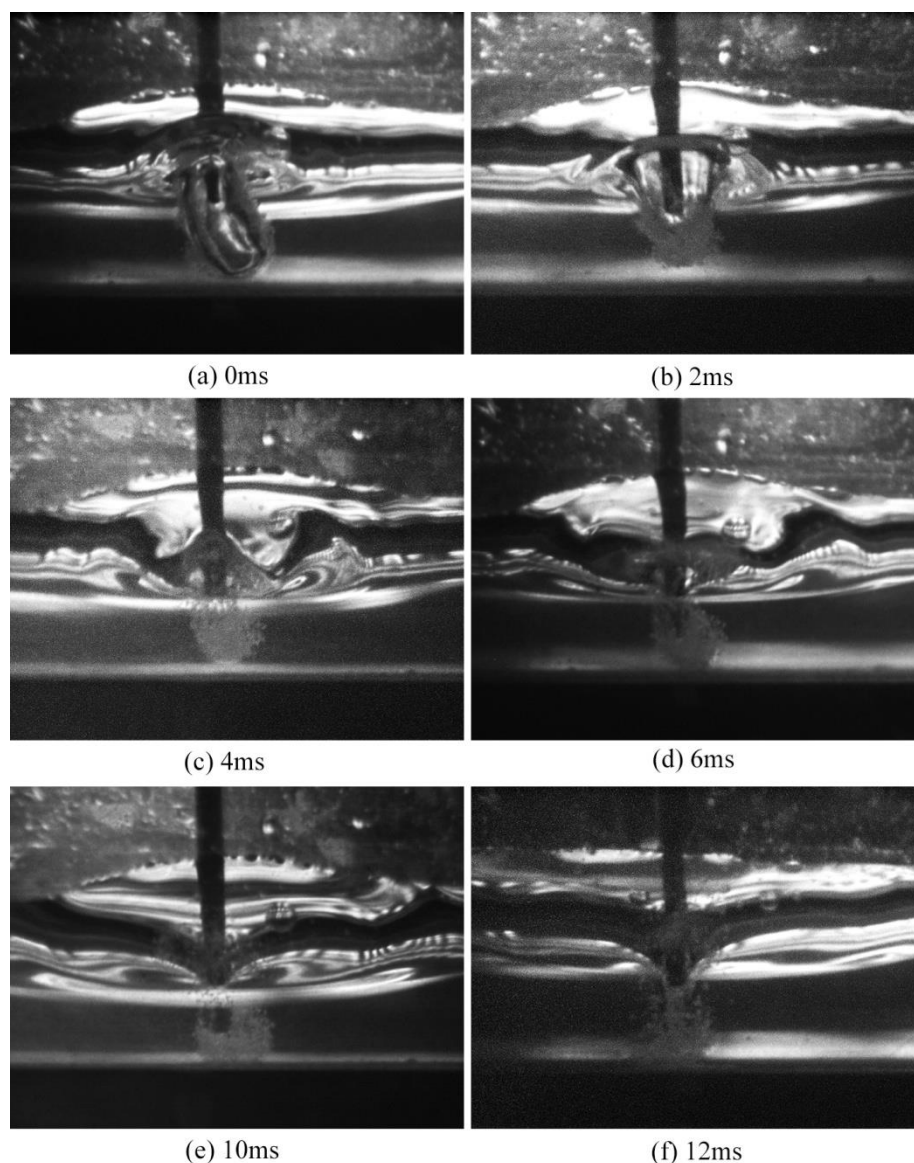


Figure 6. Formation of a complete gas film under an applied voltage of 30 V.

Once the large bubble was formed, the contact points between the electrode and electrolyte were reduced. Figure 6. (a) shows that the large bubble was almost detached from the electrode. Therefore, the large bubble isolated the electrode from the electrolyte. The corresponding current at this moment

was 310 mA, which also indicated that the contact area between the electrode and electrolyte was small. Otherwise, higher electrolysis currents would be generated. The small contact area between the electrode and electrolyte implies that the contact area between the electrode and bubble surface was also small, leading to a small surface adhesion. The large bubble was simultaneously subjected to buoyancy. As the surface adhesion was small, the large bubble began to move upwards due to the buoyancy; 2 ms later, the large bubble moved to a position just below the liquid level and had an inverted cone shape, as shown in Figure 6 (b). The corresponding current at this moment was 100 mA. Subsequently, the large bubble continued to move up and broke the liquid level, as shown in Figure 6 (c). The disturbance caused by the breaking of the liquid level spread to the surrounding as ripples, as shown in Figures 6 (c)–(f). The spread speed was calculated to be 0.42 m/s. Finally, a complete gas film was generated around the electrode, as shown in Figure 6 (h), and then the discharge stage began.

According to the above phenomena, the formation of a thin complete gas film includes two stages. At the first stage, the bubbles around the electrode coalesce into a large bubble. Subsequently, the large bubble forms a thin complete gas film due to buoyancy. In a previous study, it was supposed that the transition from a bubble layer to a gas film is attributed to bubble coalescence [6]. The observation in this study revealed that both bubble coalescence and buoyancy exerted on the bubble contribute to the formation of the gas film.

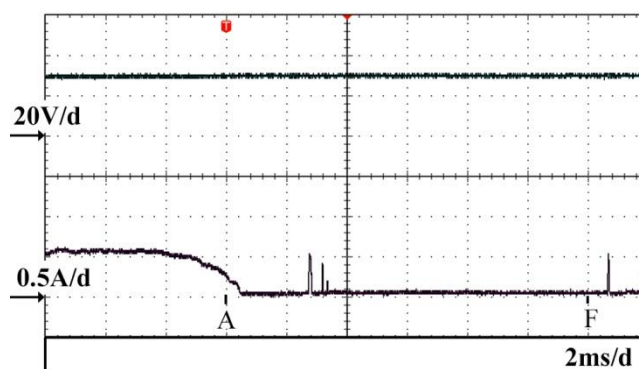


Figure 7. Voltage and current waveforms for the formation of a complete gas film.

3.3 Gas film in the discharge stage

Discharge occurs when a complete and stable gas film is produced. At the discharge stage, the stability of the gas film is affected by the discharge. When large fluctuations are applied to the gas film, they will be reflected in the current signals [26]. In the experiments, high current pulses with peak values larger than 1 A depending on the experimental parameters were produced at the discharge stage [21]. In order to reveal the nature of these current pulses, the shapes of the gas film before and after the occurrences of the current pulses were captured and effects of the current pulses on the gas film were investigated.

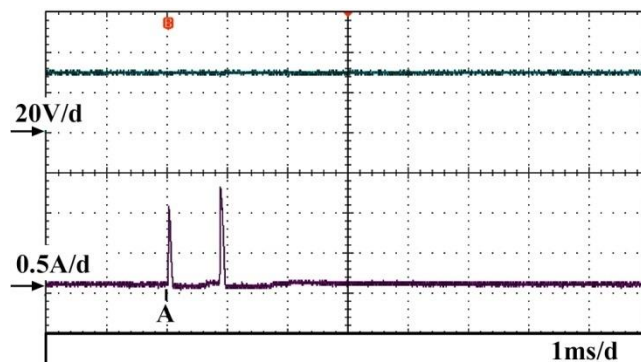


Figure 8. Two current pulses were produced during the discharge stage.

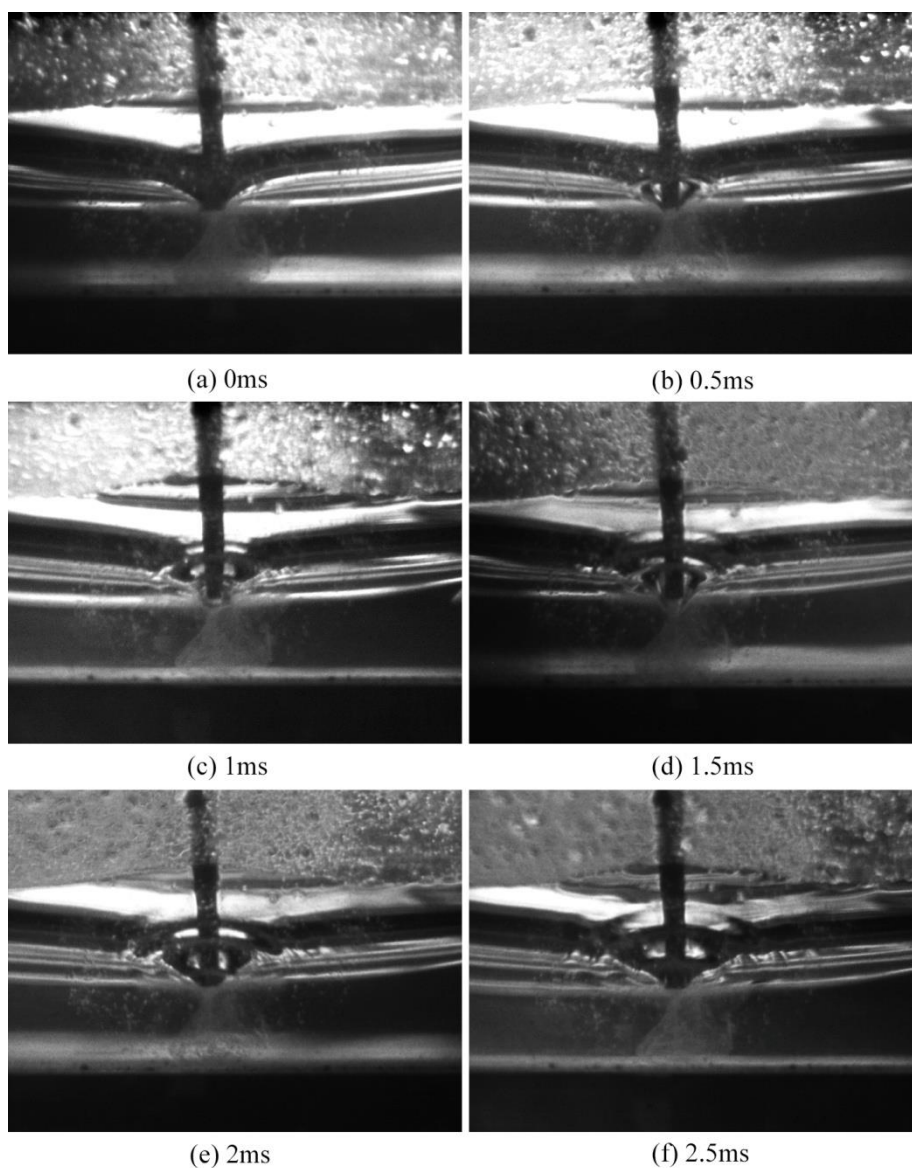


Figure 9. Gas film images when two current pulses are produced.

Figure 8 shows the voltage and current waveforms during the discharge stage under an applied voltage of 30 V. The figure shows that two current pulses are produced. The first current pulse, generated immediately after point A, has a peak value of 1.1 A and pulse duration of 80 μ s. For the second pulse, the peak value is 1.3 A, while the pulse duration is 100 μ s. The rest of the current waveform varies from 100 mA to 200 mA.

Figure 9 shows gas film images at time intervals of 0.5 ms. Point A in Figure 8 corresponds to the start of the image acquisition. At this moment, the corresponding gas film image is shown in Figure 9 (a). The gas film structure in the figure indicates that the thinnest gas film is located at the electrode tip. Therefore, the electrode tip is a position where the electrolyte is most likely to come into contact with when the gas film is disturbed. Figure 9 (b) shows that a bubble was formed at the electrode tip after the generation of the first current pulse. Figure 9 (c) shows a gas film image immediately after the generation of the second current pulse. A new bubble was formed at the electrode tip. The newly formed bubble is merged into the gas film and a ripple is produced owing to the disturbance caused by the bubble generation, as shown in Figure 9 (d). The upper ripple in the figure was caused by the first current pulse. Subsequently, the two ripples spread along the curved liquid surface and finally reached the electrolyte level, as shown in Figures 9 (e) and 9 (f).

The above observations revealed that current pulses with peak values larger than 1 A in ECDM are electrolysis currents used for the production of hydrogen gas around the tool electrode. This is consistent with an analysis in a previous study [27]. The gas bubbles produced by electrolysis merge into the gas film to form a new complete gas film.

3.4 Gas film after power switch-off

Pulse voltage was usually used as the power supply in ECDM to decrease the taper phenomenon around the hole entrance and avoid serious tool wear, as reported by Kim [28]. The periodic pulse-on–pulse-off of the applied voltage affects the shape of the gas film. The shape change of the gas film during the pulse-off stage affects the gas film structure at the subsequent pulse-on stage. The gas film evolutions during the pulse-off stage were captured by the high-speed camera, as shown in Figure 10.

Figure 10 (a) shows the gas film at a time moment when the applied voltage was just turned-off. A complete gas film is still observed around the tool electrode at this moment. Subsequently, the gas film structure began to change. 0.3 ms and 0.6 ms later, as shown in Figures 10 (b) and 10 (c), respectively, the gas film at the bottom moved upwards along the electrode due to surface tension. 0.9 ms later, as shown in Figure 10 (d), the gas film continued to move upwards leading to exposure of the lower part of the electrode to the solution. It can be measured from the figure that the length of the exposed part of the electrode was 0.93 mm. Therefore, the mean speed of the upward-moving gas film was calculated to be 1.03 m/s. The pulse-off duration of the pulse voltage in ECDM was usually set to 1 ms. Therefore, the upward movement distance of the gas film would reach 1.03 mm within the pulse-off duration. The gas film structure was almost completely destroyed during this duration, and thus the electrolysis occurred when the pulse voltage was applied again. Zheng reported that the use of an offset voltage at the pulse-off duration can effectively improve the gas film stability and thus the machining

efficiency [16], as gas bubbles can be generated at the pulse-off duration with the applied offset voltage. The generated gas bubbles protect the gas film from damage to a certain extent; the gas film stability can be substantially enhanced. Figures 10 (e) and 10 (f) show the gas film evolution after a long period of power-off. At the time of 9.6 ms after the power switch-off, no gas film existed around the electrode and the electrolyte level returned to its original state.

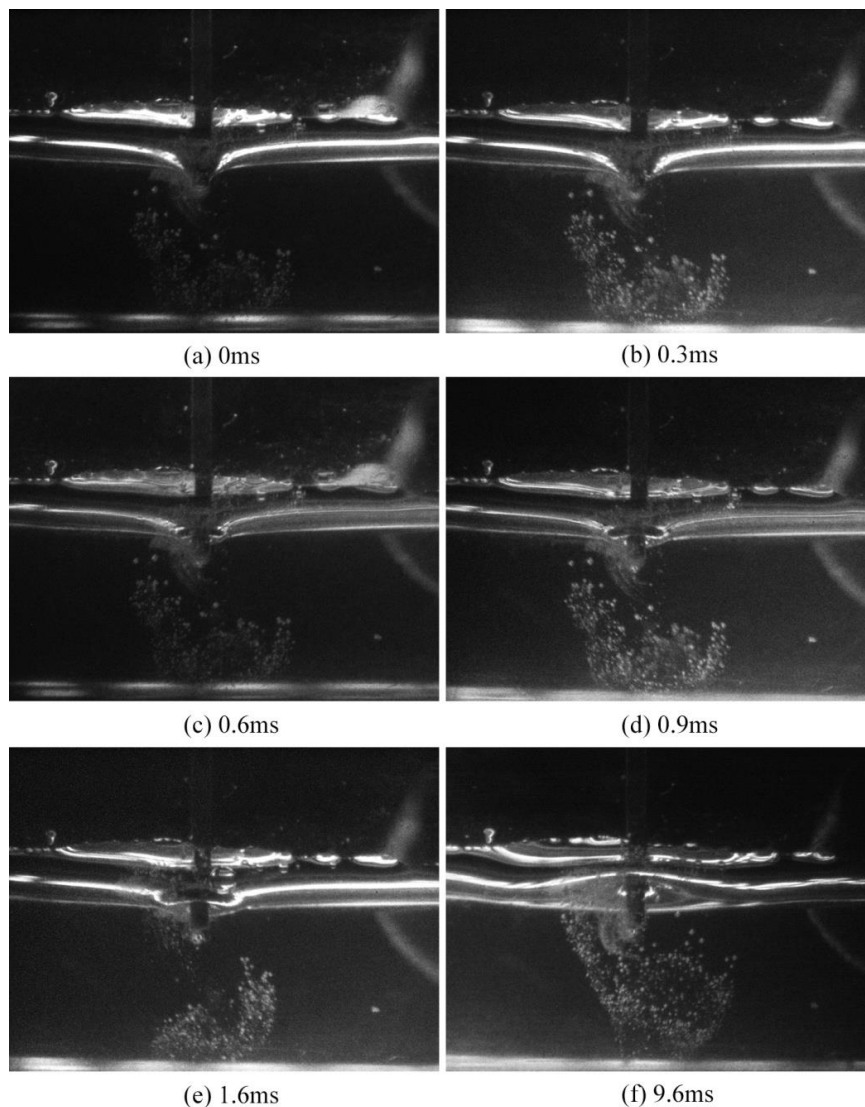


Figure 10. Gas film images after power switch-off.

4. CONCLUSIONS

A high-speed imaging technology was employed to investigate the evolution characteristics of the gas film around the tool electrode in ECDM. The captured gas film images were compared with the real-time current signals. The bubble development and bubble coalescence were observed and analysed.

Moreover, the effects of the current pulses on the gas film and evolution process of the gas film structures during the pulse-off stage were investigated. The following conclusions can be summarised:

(1) Two simultaneous processes contributed to the bubble growth. One of them was the increasing gas volume produced around the tool electrode due to electrolysis, while the other was the coalescence of the adjacent bubbles.

(2) The bubbles generated around the tool electrode first coalesced into one large bubble and then the large bubble broke through the electrolyte level due to buoyancy to form a thin complete gas film around the tool electrode.

(3) The current pulses with peak values larger than 1 A during the discharge stage were the electrolysis currents. When a current pulse occurred, a gas bubble was simultaneously produced to repair the defective gas film.

(4) The gas film evolution process during the pulse-off stage indicated that the gas film moved upwards due to surface tension; the lower part of the electrode was first exposed to the solution when the power was turned-off. The mean speed of the upward-moving gas film was calculated to be 1.03 m/s.

ACKNOWLEDGMENTS

This research was supported by the Natural Science Foundation of China (grant no. 51675341).

References

1. R. Wüthrich and V. Fascio, *Int. J. Mach. Tools Manuf.*, 45 (2005) 1095.
2. Z. P. Zheng, W. H. Cheng, F. Y. Huang and B. H. Yan, *J. Micromech. Microeng.*, 17 (2007) 960.
3. C. Yang, S. Song, B. Yan and F. Huang, *Int. J. Mach. Tools Manuf.*, 46 (2006) 2044.
4. N.S. Qu, K. Xu, Y.B. Zeng, Q. Yu, *Int. J. Electrochem. Sci.*, 8 (2013) 12163.
5. M. Weinmann, O. Weber, D. Baehre, W. Munief, M. Saumer, H., *Int. J. Electrochem. Sci.*, 9 (2014) 3917.
6. R. Wüthrich and H. Bleuler, *Electrochim. Acta*, 49 (2004) 1547.
7. V. K. Jain, P. M. Dixit and P. M. Pandey, *Int. J. Mach. Tools Manuf.*, 39 (1999) 165.
8. B. Bhattacharyya, B. N. Doloi and S. K. Sorkhel, *J. Mater. Process. Technol.*, 95 (1999) 145.
9. C. Wei, K. Xu, J. Ni, A. J. Brzezinski, and D. Hu, *Int. J. Adv. Manuf. Tech.*, 54 (2011) 987.
10. V. K. Jain, S. K. Choudhury and K. M. Ramesh, *Int. J. Mach. Tools Manuf.*, 42 (2002) 1269.
11. C. T. Yang, S. S. Ho and B. H. Yan, *Key Eng. Mat.*, 196 (2001) 149.
12. V. Fascio, R. Wüthrich and H. Bleuler, *Electrochim. Acta*, 49 (2004) 3997.
13. A. B. Kamaraj, S. K. Jui, Z. Cai and M. M. Sundaram, *Int. J. Adv. Manuf. Tech.*, 81(2015) 685.
14. R. Wüthrich, L. A. Hof, A. Lal, K. Fujisaki, H. Bleuler, P. H. Mandin and G. Picard, *J. Micromech. Microeng.*, 15 (2005) S268.
15. R. Wüthrich and L. A. Hof, *Int. J. Mach. Tools Manuf.*, 46 (2006) 828.
16. Z. P. Zheng, J. K. Lin, F. Y. Huang and B. H. Yan, *J. Micromech. Microeng.*, 18 (2008) 025014.
17. C. K. Yang, K. L. Wu, J. C. Hung, S. M. Lee, J. C. Lin and B. H. Yan, *Int. J. Mach. Tools Manuf.*, 51 (2011) 528.
18. W. Tang, X. Kang, and W. Zhao, *J. Micromech. Microeng.*, 27 (2017) 065013.
19. I. Basak and A. Ghosh, *J. Mater. Process. Technol.*, 62 (1996) 46.
20. H. Vogt, and R. J. Balzer, *Electrochim. Acta*, 50 (2005) 2073.
21. A. Allagui and R. Wüthrich, *Electrochim. Acta*, 54 (2009) 5336.
22. C. P. Cheng, K. L. Wu, C. C. Mai, C. K. Yang, Y. S. Hsu and B. H. Yan, *Int. J. Mach. Tools Manuf.*, 50 (2010) 689.
23. B. Jiang, S. Lan, K. Wilt and J. Ni, *J. Mach. Tools Manuf.*, 90 (2015) 8.

24. H. H. Kellogg, *J. Electrochim. Soc.*, 97(1950) 133.
25. V. Raghuram, T. Pramila, Y. G. Srinivasa and K. Narayanasamy, *J. Mater.Process.Technol.*, 52 (1995) 301.
26. K. R. Kolhekar and M. Sundaram, *Precis. Eeg.*, 53 (2018) 203.
27. R. Wüthrich, U. Spaelter and H. Bleuler, *J. Micromech. Microeng.*, 16 (2006) 779.
28. D. J. Kim, Y. Ahn, S. H. Lee and Y. K. Kim, *J. Mach. Tools Manuf.*, 46 (2006) 1064.

© 2019 The Authors. Published by ESG (www.electrochemsci.org). This article is an open access article distributed under the terms and conditions of the Creative Commons Attribution license (<http://creativecommons.org/licenses/by/4.0/>).